INTERFACE

royalsocietypublishing.org/journal/rsif

Research

Cite this article: Asadzadeh SS, Larsen PS, Riisgård HU, Walther JH. 2019 Hydrodynamics of the leucon sponge pump. *J. R. Soc. Interface* **16**: 20180630.
http://dx.doi.org/10.1098/rsif.2018.0630

Received: 17 August 2018
Accepted: 20 November 2018

Subject Category:
Life Sciences–Physics interface

Subject Areas:
biomechanics

Keywords:
choanocytes, flagellar vane, low Reynolds number flow, computational fluid dynamics, positive displacement pump

Author for correspondence:
Jens H. Walther
e-mail: jhw@mek.dtu.dk

THE ROYAL SOCIETY
PUBLISHING

Hydrodynamics of the leucon sponge pump

Seyed Saeed Asadzadeh[1], Poul S. Larsen[1], Hans Ulrik Riisgård[2] and Jens H. Walther[1,3]

[1]Department of Mechanical Engineering, Technical University of Denmark, 2800 Kgs. Lyngby, Denmark
[2]Marine Biological Research Centre, University of Southern Denmark, Hindsholmvej 11, 5300 Kerteminde, Denmark
[3]Computational Science and Engineering Laboratory, ETH, Zürich, Switzerland

JHW, 0000-0001-8100-9178

Leuconoid sponges are filter-feeders with a complex system of branching inhalant and exhalant canals leading to and from the close-packed choanocyte chambers. Each of these choanocyte chambers holds many choanocytes that act as pumping units delivering the relatively high pressure rise needed to overcome the system pressure losses in canals and constrictions. Here, we test the hypothesis that, in order to deliver the high pressures observed, each choanocyte operates as a leaky, positive displacement-type pump owing to the interaction between its beating flagellar vane and the collar, open at the base for inflow but sealed above. The leaking backflow is caused by small gaps between the vaned flagellum and the collar. The choanocyte pumps act in parallel, each delivering the same high pressure, because low-pressure and high-pressure zones in the choanocyte chamber are separated by a seal (secondary reticulum). A simple analytical model is derived for the pump characteristic, and by imposing an estimated system characteristic we obtain the back-pressure characteristic that shows good agreement with available experimental data. Computational fluid dynamics is used to verify a simple model for the dependence of leak flow through gaps in a conceptual collar–vane–flagellum system and then applied to models of a choanocyte tailored to the parameters of the freshwater demosponge *Spongilla lacustris* to study its flows in detail. It is found that both the impermeable glycocalyx mesh covering the upper part of the collar and the secondary reticulum are indispensable features for the choanocyte pump to deliver the observed high pressures. Finally, the mechanical pump power expended by the beating flagellum is compared with the useful (reversible) pumping power received by the water flow to arrive at a typical mechanical pump efficiency of about 70%.

1. Introduction

Grazing on phytoplankton and free-living bacteria in marine filter-feeding invertebrates implies feeding on highly dilute suspensions of food particles, and, therefore, invertebrates must process large volumes of water in highly efficient filters in order to cover their food requirements [1,2]. Thus, filter-feeding sponges filter a water volume six times [3], or higher [4], than their volume body per minute. A basic understanding of the pumping and filter mechanisms and the energy cost therefore continue to attract attention [2,4–10].

To understand the overall pump function in a filter-feeding organism, it is common practice to consider the pump and system characteristics expressed by pressure change P versus water flow rate Q [2]. Thus, as a pump faces an increase in pressure head, the flow generally decreases as given by the pump characteristic $P_p(Q)$. On the other hand, the system pressure drop owing to friction through canals and restrictions increases with increasing flow as given by the system characteristic $P_s(Q)$. The intersection between the two relations defines the operating point, and the pressure head at this point is termed the normal operating pump pressure (cf. for example [2, fig. 1], [8, fig. 14.6]). None

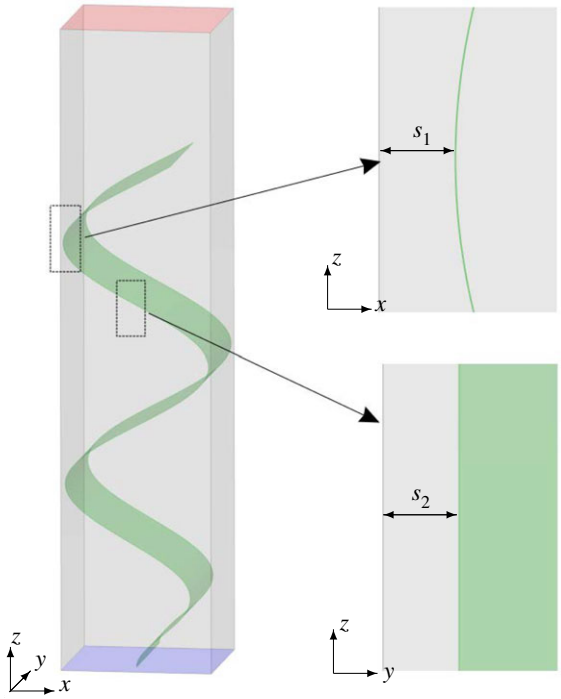

Figure 1. Conceptual collar–vane–flagellum model. Flagellar vane (green) inside a sealed collar of 3.1 µm square cross section and height 13.2 µm (grey) with inlet (blue), outlet (red) and defined gaps s_1 and s_2 for flow leaks between the beating flagellum edges and the collar. (Online version in colour.)

of these characteristics has so far been measured directly in an organism but they can be estimated from models. However, the so-called back-pressure characteristic $P_b(Q)$ may be determined experimentally by measuring the flow Q for increasing values of back-pressure P_b imposed at the exhalant flow from the organism. Adding an estimated system characteristic to a measured back-pressure characteristic gives the pump characteristic, which was done by Larsen and Riisgård [7] for the marine demosponge *Haliclona urceolus*. Despite the linearity of the governing equations of the flow in the low Reynolds number regime inside the canal system, the measured back-pressure characteristic was found to be nonlinear. These authors suggested that changes in the diameter of the elastic inhalant and exhalant canals with changes in local hydrostatic pressure might explain the curved back-pressure characteristic. However, the leaky positive displacement pump model presented here also leads to a curved model-pump characteristic owing to increased leakage in the pump in response to increasing pressure.

Further, noting the high back-pressure at zero flow (about 2.7 mmH_2O) and high inferred normal operating pump pressure (0.673 mmH_2O) [7] suggested that the choanocyte chamber in demosponges was the basic pump unit, acting as a leaky positive displacement pump due to a constructive interaction between the long flagella of the many choanocytes in the chamber, but this may be erroneous for several reasons. Video recordings [10] have shown that the flagella beat asynchronously and at different frequencies, hence excluding coordinated interaction. Also, the structure of the choanocyte chamber with a low- and a high-pressure zone [9–11] suggests that all choanocytes at the distal part of the collars are exposed to the same pressure. In the present study, the positive displacement mechanism is suggested to be at play in the collar of each choanocyte, which is therefore suggested to be the basic pump unit, and these units act independently in parallel, each delivering the full pressure required to drive the flow.

In asconoid and syconoid body-type sponges [12] where choanocytes line walls, they appear to work in parallel and are therefore the basic pump units. They deliver the moderate pressure rise required to draw water through the inhalant openings (ostia) and to maintain flow through the rather short and open canals and the exhalant openings (oscula) of these species. In leuconoid-type sponges, choanocytes may still be the basic pump units now lining the walls of choanocyte chambers. But because of the much higher pressure required to drive flow through the longer and more complex system of canals, the choanocyte chambers are designed with sealed zones of low pressure and high pressure [9–11]. The pressure rise between these zones is maintained by the action of vaned flagella essentially functioning as leaky positive displacement pumps in the collars with well-spaced microvilli near the cell but essentially sealed microvilli by a mesh of glycocalyx in the upper part of the collar [9–11].

As noted by Mah *et al.* [10] the collar–flagellum system should be seen as a functionally integrated unit and an integrated collar–vane–flagellum system would require more complex modelling than, for example, slender body theory traditionally used in describing choanoflagellate propulsion or pumping by a beating flagellum. We support this view in the present modelling of the leucon sponge pump.

We first derive a simple analytical gap model which is verified by results from computational fluid dynamics (CFD) applied to a conceptual model of the collar–vane–flagellum system. This model is subsequently used to derive the pump characteristic by imposing an estimated system characteristic to finally obtain the back-pressure characteristic that is compared with available experimental data. The CFD model is then extended to a choanocyte model representing a unit section of the choanocyte chamber holding one choanocyte to study the effects of different elements of the choanocyte pump on its functionality.

2. Material and methods

In this section, we first describe the numerical approach for studying the flow in choanocyte models. Next, we explain the theory for the gap and the pump model.

2.1. Computational fluid dynamics

We use CFD to numerically solve the governing Navier–Stokes equations of the fluid dynamics in both the conceptual collar–vane–flagellum model and a choanocyte model. A finite volume method is used to discretize and solve the equations on a discrete representation of the computational domain consisting of polyhedral cells (electronic supplementary material, figure S1) by applying the commercial CFD code STAR-CCM+(13.02.011-R8).

2.1.1. Governing equations

The governing equations of an incompressible Newtonian fluid with density ρ and viscosity μ are the continuity and Navier–Stokes equations,

$$\nabla \cdot \mathbf{u} = 0 \tag{2.1}$$

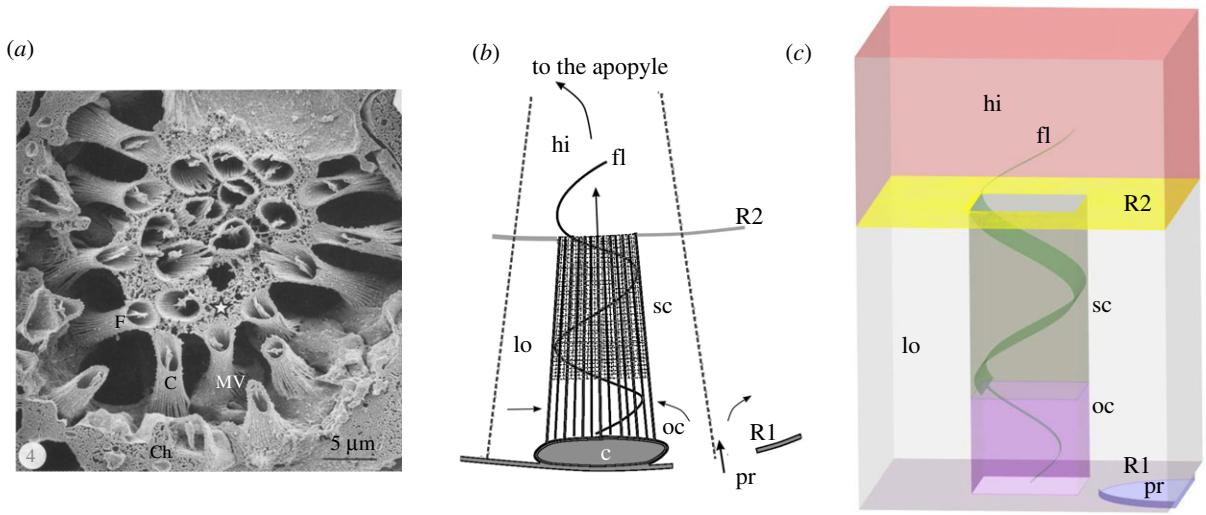

Figure 2. Choanocyte chamber and model. (*a*) Scanning electron microscope (SEM) image of the choanocyte chamber of the freshwater sponge *Spongilla lacustris*. Choanocyte (Ch), microvilli (MV) of collars, flagellum with vane (F), ends of collars (C) connected to the secondary reticulum (*). Reproduced with permission from [11] (license no. 4464811172505). (*b*) Schematic of a unit section of the choanocyte chamber holding one choanocyte. Cell (c); flagellum (fl); collar, open near cell (oc), sealed by glycocalyx mesh above (sc), and connected to other collars at distal ends by a sealed secondary reticulum (R2) bounding the high-pressure zone (hi). Arrows show inflow from the incurrent canal system through the prosopyle (pr) to the low-pressure zone (lo) bounded by the primary reticulum (R1) and through the opening at the collar base (oc). Stippled lines represent the surface between adjacent similar domains, each with one choanocyte. The flow from the many (50–80) choanocytes in the chamber leaves the high-pressure zone through a single outlet, the apopyle (not shown), leading to the excurrent canal system. (*c*) Choanocyte model used in the CFD study where different boundary conditions (table 1) are imposed on surfaces between adjacent choanocytes to simulate possible interactions between neighbouring choanocytes. The computational domain consists of a 3.1 µm square by 8.2 µm high collar centred in a 9 µm square by 13.2 µm high outer domain with a semi-circular prosopyle inlet of diameter 5 µm at lower right. (Online version in colour.)

and

$$\rho\left(\frac{\partial \mathbf{u}}{\partial t} + (\mathbf{u}\cdot\nabla)\mathbf{u}\right) = -\nabla p + \mu\nabla^2\mathbf{u}, \tag{2.2}$$

where $\mathbf{u}$ and p denote the velocity and pressure, respectively. In the small-scale world of choanocytes the Reynolds number, the ratio of inertia to viscous forces, is small; here $\mathrm{Re} = \rho VL/\mu = 5.7 \times 10^{-4}$, where $\rho = 997\ \mathrm{kg\ m^{-3}}$, $\mu = 0.001\ \mathrm{Pa\ s}$, and $L = 10.4\ \mu\mathrm{m}$ is the flagellar central length and $V = \lambda f$ is the wave speed, in which $f = 11.0\ \mathrm{Hz}$ is the frequency and $\lambda = 5\ \mu\mathrm{m}$ is the wavelength [10]. Therefore, the left-hand side of equation (2.2) is negligible, and the flow can be considered as quasi-steady.

We model the displacement of the flagellum in the x direction as a simple travelling wave,

$$d(z,t) = a(1-e^{-z})\sin\left(\frac{2\pi}{\lambda}(z - Vt)\right), \tag{2.3}$$

where d is the lateral displacement of the flagellum, a is the amplitude, z is the centreline axis of the collar and t is time. With this model, the flagellar length varies slightly in time during the beat cycle (a maximum of 1.6%). And since the flow is quasi-steady, the variation in length depends only on two successive positions of the flagellum, which is significantly smaller (~0.02% with a time step $\delta t = 0.0001\ \mathrm{s}$ between two successive positions of the flagellum).

The power expenditure by the vaned flagellum is calculated as

$$\mathcal{P} = \int\int_{S_{\mathrm{fl}}} \mathbf{u}\cdot(\sigma\cdot\mathbf{n})\,\mathrm{d}S, \tag{2.4}$$

where $\sigma = -p\mathbf{I} + \mu(\nabla\mathbf{u} + (\nabla\mathbf{u})^{\mathrm{T}})$ denotes the stress tensor, $\mathbf{n}$ is the unit normal vector on the surface S pointing into the fluid and S_{fl} is the flagellar vane area.

2.1.2. Collar–vane–flagellum model

The key to delivering a relatively high pressure (in order to drive flow through the narrow canals in sponges) lies in the collar–vane–flagellum system that effectively functions as a leaky pump. For the conceptual study of the effect of gap size on the maximum pressure delivered by the flagellum pump, we replace the cylindrical collar of the circular cross section (3.1 µm diameter) by one of square cross section (3.1 µm width). This model provides well-defined gaps s_1 and s_2 between the beating flagellar vane edges and the collar (figure 1). The flagellar vane is modelled as a plate beating in a plane subject to a no-slip boundary condition relative to the motion of the flagellum. The sides (collar) of the computational domain are subject to the no-slip condition, and the inlet and the outlet to pressure boundary conditions representing the imposed system pressure losses associated with flow through restrictions and canals in the sponge.

2.1.3. Choanocyte model

The choanocyte chamber holds a large number of choanocytes (figure 2*a*) in a close-packed array on its nearly spherical inner wall (primary reticulum) [4,11]. Our simplified choanocyte model for CFD studies (figure 2*c*) is based on the description in [11]. Here, figure 2*a* shows the choanocyte chamber in the freshwater demosponge *Spongilla lacustris* and figure 2*b* shows a schematic of a unit section of the choanocyte chamber holding one choanocyte. In *S. lacustris*, the average collar length is ~8.2 µm and the collar has 24–36 microvilli of diameter ~0.12 µm and spacing ~0.06 µm at their base [10,13]. The microvilli over the distal two-thirds of the collar are tightly held together with a glycocalyx mesh [9,10]. Despite variations in the collar length and the number of choanocytes, the microvilli and the glycocalyx mesh are believed to be similar among many species of sponges [4,9–11,14].

Inflow through a sponge body is driven by suction through numerous small openings (ostia) in its outer surface and further through incurrent canals to enter the choanocyte chambers through several prosopyles before it reaches the choanocyte collars [4,9]. The choanocyte pumps provide the suction for inflow and further the pressure for the subsequent outflow from the choanocyte chambers through the apopyle and excurrent

canals to the exit at the osculum. Inside the flagellated collar chamber, the water is sucked through the relatively large openings between the microvilli at the base of the collar (marked 'oc' in figure 2*b*) and its pressure then increases in the mesh-sealed part of the collar (marked 'sc' in figure 2*b*) by the beating flagellum on its way into the the inner region of the chamber. This is possible because a low-pressure zone is established between the primary and secondary reticula (R1 and R2, respectively; figure 2*b*) and a high-pressure zone between the secondary reticulum and a cone cell ring (near the apopyle, not shown). The secondary reticulum consists of a rather dense, mucus-like material [11,15]. This arrangement implies that all choanocytes within a chamber experience and hence deliver the same pressure head. Therefore, it is sufficient to simulate a unit section of the choanocyte chamber holding one choanocyte and subsequently account for possible interactions with neighbouring unit sections by applying various appropriate boundary conditions on the surface of such a unit section.

In the choanocyte model used for the CFD simulations (figure 2*c*), the flagellum (green) beats with an amplitude of 1.5 µm, has a 3 µm vane only along the sealed part of the collar while it is unvaned and of width 0.3 µm over the rest of its length, as observed by [10,16]. But we also model the flagellum as vaned over its full length to study its effect on the pump performance. The cross section of the collar is the same as given in figure 1. The proximal 2.1 µm length of the collar with opening (oc) is modelled as a porous surface with an assigned porosity corresponding to that of a network of parallel and equidistantly spaced cylinders [17]. The distal fine-meshed part of the collar (sc) is treated as an impermeable surface, but cases of a semipermeable surface [18,19] are also considered to study the effect of the mesh pore size on the pump performance. Primary and secondary reticula (R1 and R2) are modelled as impermeable surfaces subject to the no-slip condition. A pressure boundary is imposed on the outer surfaces representing the high-pressure zone (red). The other four sides of the outer domain (light grey) are exposed to different boundary conditions, i.e. pressure, periodic, symmetry, to model different scenarios of interaction between unit sections. The last two cases, for example, represent a colony of choanocytes with flagella beating in phase or completely out of phase, respectively. The prosopyle is a semi-circle with a diameter of 5 µm subject to either a pressure boundary, to represent choanocytes sitting near the prosopyle, or a no-slip boundary (i.e. closed), to represent those sitting far from the prosopyle.

2.2. Theory

2.2.1. Leak flow through gaps

To relate the leak flow to pressure rise and widths of the gaps, we consider the collar–vane–flagellum system presented in figure 1. The net volume flow Q of the leaky pump is the difference between the positive displacement flow Q_{pos} and the negative leak flows through the gaps,

$$Q = Q_{\mathrm{pos}} - (Q_{s_1} + Q_{s_2} - Q_{s_1,s_2}), \tag{2.5}$$

where $Q_{\mathrm{pos}} = \lambda f(W - 2s_1)(W - 2s_2)$ and W is the square collar width, Q_{s_1} and Q_{s_2} are the leak flow through the gaps of width s_1 and s_2, respectively, and Q_{s_1,s_2} is the leak flow through overlapping areas where the two gaps meet in the corners of the collar.

The leak flow depends on the excess pressure P generated by the positive displacement effect and the width of gaps between the flagellum and the collar. For an estimate of the leak flow through the gap width s_i (Q_{s_i}, i = 1, 2), consider the leak to be fully developed laminar flow between two parallel plates of spacing s, length l and width w ($s \ll w$) for which the frictional pressure drop is $P = 12\mu Ul/s^2$ [2,20]. Here, U denotes the mean velocity that is related to leakage by $Q_s = swU$, yielding the relation

$$Q_s = \frac{Pws^3}{12\mu l} \simeq cs^2P, \tag{2.6}$$

where we have assumed a geometric scaling in which $s/l \simeq$ const., which along with other constant parameters are lumped into the constant c. For an estimate of Q_{s_1,s_2} we use the pressure drop expression for an orifice of diameter r ($Q_r = 24\mu P\, r^3$) [21] and assume the same order of magnitude gap widths ($s_1 \sim s_2$),

$$Q_{s_1,s_2} \simeq c_3 s_2^3 P, \tag{2.7}$$

where c_3 is a constant. Using equation (2.6) for the leak flow through the gap width s_i (Q_{si}) and combining it with equations (2.5) and (2.7), in the shut-off condition of no net flow ($Q = 0$), gives

$$P_{\max} = \frac{\lambda f(W - 2s_1)(W - 2s_2)}{c_1 {s_1}^2 + c_2 {s_2}^2 - c_3 s_2^3}, \tag{2.8}$$

where c_1 and c_2 are constants corresponding to gap widths s_1 and s_2, respectively.

2.2.2. Leaky positive displacement pump model

To derive a simple model for the pump characteristic, we assume one and the same small gap size in both directions (figure 1 with $s_1 = s_2 = s \ll W$) or, as a special case, contact between the flagellum and the collar in one direction at all times ($s_1 = 0$, $s_2 \neq 0$). Using equations (2.5) and (2.6) (neglecting the third-order term of equation (2.7)), the leaky positive displacement choanocyte pump, consisting of a vaned flagellum beating in the sealed part of the collar, delivers a net volume flow rate of

$$Q = Q_{\mathrm{pos}} - Q_{\mathrm{leak}} \simeq \lambda fA - \alpha_s s^2 P, \tag{2.9}$$

where A is the cross sectional area of the collar and α_s is a constant. Note that, in the case of a cylindrical collar, the gap shape within the collar is more complex and the gap width might vary inside the collar. Assume a gap shape $s(h)$ as a function of arc length h along the flagellum edges. Now $\mathrm{d}Q_{s(h)} = c_s \mathrm{d}h\, [s(h)]^2\, P$ defines the leak for a segment length dh. For the total leak flow, we have

$$Q_{\mathrm{cyl,leak}} = \int_0^H \mathrm{d}Q_{s(h)} = \alpha\left(\frac{1}{H}\int_0^H [s(h)]^2 \mathrm{d}h\right)P, \tag{2.10}$$

where H is the total arc length along the flagellum edges, and $\alpha = c_s H$ is a constant. Hence, for a cylindrical collar equation (2.9) is still valid but the gap width s should be replaced by the root mean square of the varying gap $s(h)$.

It is furthermore expected that the gap width s will increase with increasing pressure owing to linear elastic deformation of the flagellar vane and/or the collar according to

$$s - s_o = \frac{P}{k}, \tag{2.11}$$

where k is an elastic modulus and s_o denotes the minimum gap width at zero pressure. Inserting equation (2.11) into equation (2.9) gives the equation for the model pump characteristic

$$Q = Q_{\mathrm{pos}} - \alpha_s P\left(s_o + \frac{P}{k}\right)^2, \tag{2.12}$$

or in normalized form in terms of pump pressure head $P = P_{\mathrm{pump}}$, satisfying the conditions of $Q(P_{\mathrm{pump}} = 0) = Q_o$ and $P_{\mathrm{pump}}(Q = 0) = P_o$,

$$Q = Q_o\left\{1 - \frac{P_{\mathrm{pump}}}{P_o}\left(C_1 + (1 - C_1)\frac{P_{\mathrm{pump}}}{P_o}\right)^2\right\}, \tag{2.13}$$

where $C_1 = s_o/(s_o + P_o/k)$ is a constant.

3. Results and discussion

In this section, we first present the results of the conceptual flagellum–vane–collar system. Next we compare the derived pump model with experimental data, and finally examine detailed CFD results obtained with the choanocyte pump model in regard to the functionality of the pump.

3.1. Effect of gap sizes on pressure rise

To study the gap size effect, we perform CFD simulations of the collar–vane–flagellum system (figure 1) for the 'shut-off' condition (closed inlet and outlet) to obtain the maximum pump pressure versus changes in gap widths s_1 and s_2. As shown in figure 3, the 16 points obtained from the CFD simulations show very good agreement with the analytical model (equation (2.8)). The three constants c_1, c_2 and c_3 in equation (2.8) are found by using three arbitrary points from the CFD results. The pressure depends strongly on gap sizes and it decreases dramatically as gaps become larger. This also indicates that an unvaned flagellum would be unable to generate the required pressure due to the huge gap between the flagellum and the collar.

Note that equation (2.8) gives the maximum pressure delivered by the leaky pump for a rigid flagellum and a rigid collar with an asymptotic infinite pressure as the gap widths decrease to zero (figure 3). Although the vane in choanoflagellates is a delicate structure, the vane in choanocytes appears 'dense and massive' [16], but nevertheless the flagellar vane and/or the collar are still deformable and likely to bend or expand, resulting in gaps of increasing widths if the pressure load increases sufficiently. Therefore, the actual maximum pressure that a flexible flagellum–vane–collar system is able to deliver will remain finite.

3.2. Sponge pump

To test the leaky pump model (equation (2.13)) against experimental data, we consider the measured back-pressure data of the marine demosponge *Haliclona urceolus* [7, fig. 1c and table 1]. To obtain the model back-pressure characteristic, we subtract the system characteristic from the model-pump characteristic (equation (2.13)). The system characteristic is obtained from the estimated system pressure losses given in table 1 of [7] for the 'standard sponge' of [6], with a modified value for the pressure drop in the collar slits. Since the collar is sealed over the distal two-thirds of its length [10], and the flow only passes through the collar slits at the proximal part, the velocity and hence the table value of pressure drop through the slits are increased by a factor of 3 to give a total of $0.7596 + 0.1576 = 0.9172\ \mathrm{mmH_2O}$ at the operating point of the 'standard sponge' in table 1 of [7]. Noting that the contribution from the kinetic energy of exhalant jet from the osculum is quadratic in velocity (or volume flow) while other contributions are linear, and that values correspond to an operating point (zero back-pressure) of $Q_{\mathrm{op}} = 6\ \mathrm{ml\ min^{-1}}$, we scale to the present case of $Q_{\mathrm{op}} = 4.96\ \mathrm{ml\ min^{-1}}$ (read from measured zero back-pressure) by the expression [7]

$$P_{\mathrm{s}} = \frac{0.628Q}{Q_{\mathrm{op}}} + 0.108\left(\frac{Q}{Q_{\mathrm{op}}}\right)^2. \tag{3.1}$$

To plot the modelled pump characteristic of equation (2.13), the parameter $P_o = 2.69\ \mathrm{mmH_2O}$ is taken from the measured

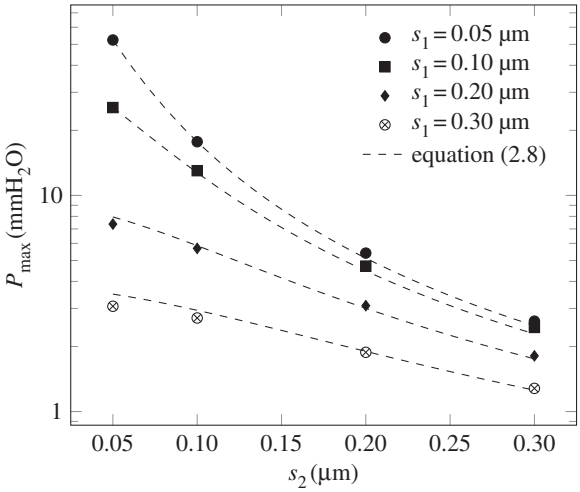

Figure 3. Effect of gap widths s_1 and s_2 on the maximum pressure delivered by the flagellum–vane–collar system (figure 1) under the 'shut-off' condition of closed inlet and outlet. Equation (2.8) (dashed curves) fits well the CFD results (symbols). The pressure rise highly depends on the gap sizes and thus on the flagellum–collar interaction.

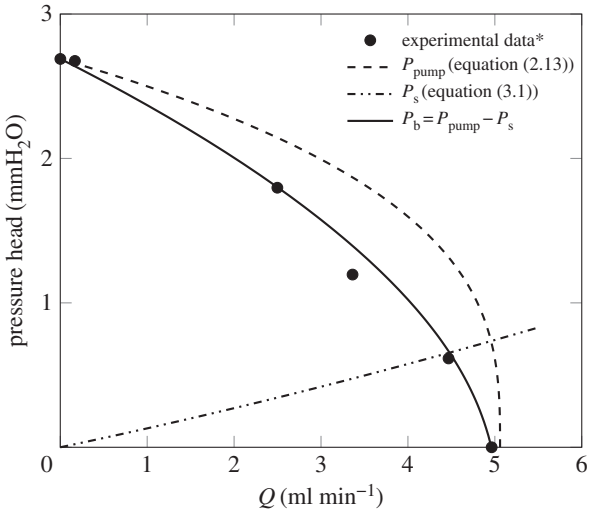

Figure 4. Modelled pump characteristic (P_{pump}, obtained from equation (2.13) with $C_1 = 0$, dashed) minus estimated system characteristic (P_{s}, equation (3.1), dashed-dot) gives resulting back-pressure characteristic (P_{b}, solid) in good agreement with experimental data (symbols). *[7, fig. 1c].

shut-off pressure head at $Q = 0$, and the parameter $Q_o \simeq 5.07\ \mathrm{ml\ min^{-1}}$ is obtained by employing the operating condition ($P_{\mathrm{s,op}}$, Q_{op}) in equation (2.13). Figure 4 shows the back-pressure experimental data, the system characteristic (P_{s}) from equation (3.1), the model-pump characteristic (P_{pump} with $C_1 = 0$ in equation (2.13) corresponding to the zero gap at zero pressure) and the resulting back-pressure characteristic (P_{b}). The modelled back-pressure characteristic captures the general trend of the experimental data.

It can be seen from figure 4 that flow rate Q_{op} at the operating point lies very close to the maximum flow rate (Q_o), indicating a minimal leakage from the pump units of about 2%, as reflected by the steepness of the pump characteristic. Thus, the pump continues to operate almost at its full potential (at a given frequency) with minimal leakage for an increase to system pressure losses in the range from 0 to $0.736\ \mathrm{mmH_2O}$.

As an estimate of the maximum flow rate per individual choanocyte, i.e. the positive displacement flow ($Q_{\mathrm{pos}} \simeq \lambda f A$),

Table 1. Flow rate (Q) and power expenditure ($\mathcal{P}$) by a partial and full flagellar vane for four different boundary conditions (BCs) on the choanocyte model (figure 2*c*), subject to an imposed pressure head of 1 mmH_2O. (1) Specified inlet pressure on sides, (2) periodicity on sides, (3) symmetry on sides, (4) specified inlet pressure on sides with no prosopyle. The hydrodynamic interaction between adjacent choanocytes is negligible, and the full flagellar vane does not increase flow rate significantly, as compared with the partial flagellar vane, but is energetically more demanding.

	partial flagellar vane		full flagellar vane	
BC	Q ($\mu m^3\ s^{-1}$)	$\mathcal{P}$ (fW)	Q ($\mu m^3\ s^{-1}$)	$\mathcal{P}$ (fW)
1	454	12.6	456	14.2
2	453	12.6	456	14.3
3	453	12.6	456	14.3
4	454	12.6	456	14.2

we use the dimensions for *S. lacustris* choanocytes [10, table 1]. Employing the mean value of collar width at the collar base (3.1 µm) and the collar angle (−5°), the collar width at its tip is ∼1.67 µm, resulting in a flow rate of $Q_{pos} \sim 0.43 \times 10^{-6}$ ml h^{-1}. This value is similar to the mean flow rate per choanocyte for different species of both glass sponges and demosponges (table 2), obtained from measured volume flow rate (per ml sponge) divided by the number of choanocytes per mm^3 [4]. This suggests that choanocytes as the basic pumping units are functionally similar among different species and the positive displacement pumping rate appears to be a realistic approximation of the mean flow rate of a choanocyte. Nonetheless, the exact pumping rate per individual choanocyte might still vary even among those inside the same chamber as a result of observed variations in both beat frequency (ranging from 3.2 to 20.9 Hz for *S. lacustris*) and dimensions of the collar [10].

3.3. Choanocytes in chamber

In this section, using the choanocyte model of figure 2*c*, we present results of CFD simulations of the flow in and around the choanocyte of *S. lacustris* as a model organism, discuss the possible interaction among adjacent choanocytes, and study the influence on pump performance of the glycocalyx mesh and of the secondary reticulum (R2).

3.3.1. Choanocyte interactions

To examine the possible hydrodynamic interaction between adjacent choanocytes exposed to the same pressure load, we measure the flow rate and the power required for the pumping under different scenarios obtained by applying different boundary conditions on the outer boundary of the solution domain in figure 2*c*.

Table 1 lists the results for four different boundary conditions (BCs) for two cases, i.e. the normal one, where the vane of the flagellum exists over the length of the distal part of the collar (partial), and the hypothetical one, where the vane exists along the full length of the flagellum (full). The results are for an imposed pressure difference of 1 mmH_2O between the inlet and the outlet of the domain.

Table 2. Mean volume flow rate (Q_{ch}) per choanocyte for different species of demosponges and one species of glass sponge (*Aphrocallistes vastus*). Data obtained from measured volume flow rate divided by the number of choanocytes, both per unit volume of sponge [4, tables 1 and 2], *[9, table 3] and **[7, table 1]. For comparison, for demosponge *Spongilla lacustris*, the mean volume flow per choanocyte is calculated as $Q_{pos} \simeq 0.43 \times 10^{-6}$ ml h^{-1}.

species	Q_{ch} (ml h^{-1}) × 10^6
Cliona delitrix	0.22 ± 0.01
Callyspongia vaginalis	0.85 ± 0.13
Tethya californiana	0.06 ± 0.01
Haliclona mollis	0.35 ± 0.03
Neopetrosia problematica	0.36 ± 0.06
*Aphrocallistes vastus**	0.51 ± 0.34
*Haliclona urceolus***	0.20 ± −

For both cases of partial and full flagellar vane, there is no change in either flow rate or power, regardless of the in-phase (BC 2) or completely out-of-phase (BC 3) flagella beat, as compared with the reference case (BC 1), indicating negligible hydrodynamic interactions between adjacent choanocytes. The results are also unaltered for those choanocytes sitting far from the flow inlet through a prosopyle, in which case we let water enter through the lower sides into the domain (BC 4). The interaction is expected to be weak since the part of the flagellum responsible for the pressure rise lies within the distal part of the collar that is tightly held together and sealed with the glycocalyx mesh, hence to a large extent isolating this pumping region from the neighbouring ones. The lack of hydrodynamic interaction might be one reason why the beats of the flagella within a given chamber are not synchronized [10].

Additionally, a full flagellar vane does not significantly change the volume flow rate as compared with the partial flagellar vane. This is not surprising since the free part of the flagellum cannot produce any pressure rise when not beating in a sealed collar; instead, it dissipates the energy by stirring the flow in a very viscous environment. Thus, in view of the non-negligible increase in power expenditure (by about 13%) and no gain in pumping rate it makes functional sense that the vane does not extend beyond the collar filter [16] while (as another benefit) 'it appeared to narrow or be absent' towards the base of the flagellum [10]. Likewise, since the vaned flagellum and collar interaction takes place only in the distal sealed part of the collar, the first contact (or small gap) between the flagellum and collar is expected to be where the glycocalyx mesh begins. This feature has been reported by [10] for choanocytes of *S. lacustris*.

3.3.2. Effect of glycocalyx mesh

Thus far, we have treated the fine-meshed part of the collar as impermeable to flow. But how vital is the presence of the glycocalyx mesh and how dense should it be?

To answer these questions, we first simulate the choanocyte model (figure 2) subject to an imposed canal system pressure loss of $P_{ch} = 1$ mmH_2O (i.e. total pressure loss excluding contributions from within choanocyte chambers), modelling the distal part of the collar with the same

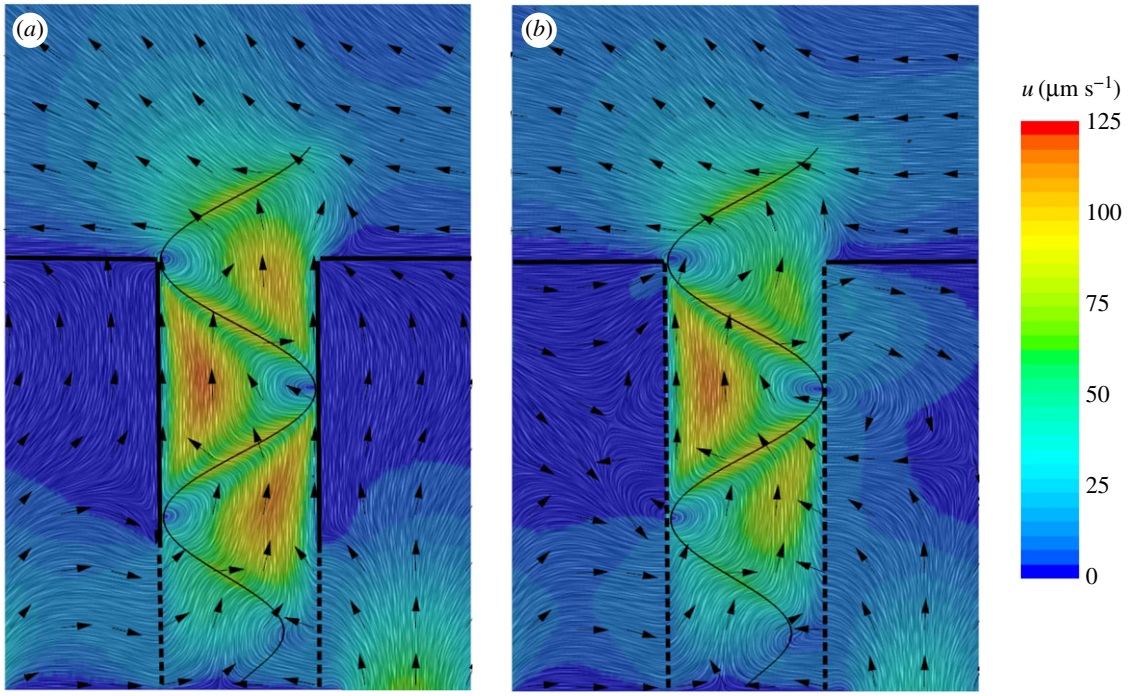

Figure 5. Velocity fields in the choanocyte model (figure 2*c*) with (*a*) and without (*b*) the presence of the glycocalyx mesh on the distal two-thirds length of the collar, for the case of an imposed canal system pressure loss of $P_{ch} = 1$ mmH_2O. With the mesh, the flow enters the collar at its base, and, after its pressure increases inside the sealed part of the collar, it leaves the collar toward the apopyle. Without the mesh, some flow leaks out through the distal part of the collar, reducing the net pumping rate as seen from the reduced inflow through the prosopyle at the lower right (see also figure 6). The colour bar and arrows (constant length) show the magnitude and direction of the velocity field, respectively. (Online version in colour.)

permeability as that of the microvilli array in the proximal part of the collar. Figure 5 shows the velocity fields for cases with and without the presence of the glycocalyx mesh. With the mesh, water enters through the base of the collar, then its pressure increases in the fine-meshed part of the collar, and it enters the inner high-pressure zone above the secondary reticulum (R2 in figure 2*c*). Without the mesh, a portion of water entering the collar from the base leaks out from the distal part rather than flowing into the high-pressure zone above the reticulum, thus reducing the net pumping rate (figure 6). Therefore, the primary hydrodynamic function of the glycocalyx mesh is to seal the distal part of the collar to prevent leakage while allowing the water to be pressurized in order to ultimately flow through the canal systems of the sponge. In the low Reynolds number regime of flow in flagellated chambers, this sealing is of paramount importance since, with the lack of inertia, the flow is pressure driven only. Besides the hydrodynamic function, the mesh also provides support against the pressure forces from within the collar to prevent a possible deformation or spreading of the microvilli.

Next, to account for possible leaks through the glycocalyx mesh, we model the fine-meshed distal part of the collar as a permeable structure composed of two layers of ~0.024 µm filaments with a pore size of ~0.045 µm [9,10]. This may be a conservative estimate of the density because of the very small spacing between the microvilli in this region [10,11].

Figure 6 presents the volume flow rate for different levels of imposed pressure and for three cases of permeability of the distal part of the collar, i.e. impermeable, with the glycocalyx mesh, and microvilli without a mesh. When the pressure load is negligible, the flow rate is independent of the permeability. But as the pressure resistance increases, the beneficial effect of the glycocalyx mesh becomes evident; here the pump can

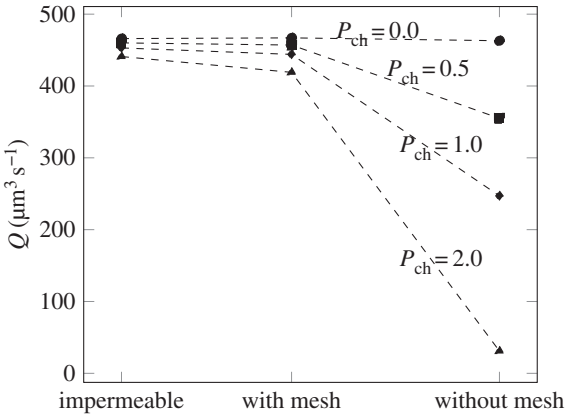

Figure 6. Volume flow rate (Q) versus permeability of the collar for different values of imposed canal system pressure loss P_{ch} (mmH_2O). For $P_{ch} = 0$, the volume flow rate is constant. For increasing values of imposed system pressure loss, the fine glycocalyx mesh is essential for the pump to deliver the required flow rate.

handle any pressure load with little change in delivered flow rate. System pressure losses from canals vary among sponges (table 3) and may also vary within a given sponge body because of different locations of choanocyte chambers and various sizes of incurrent and excurrent canals [22]. Despite the conservative estimate of the permeability of the glycocalyx mesh, it is seen to act as an almost impermeable surface. It may also be noted that a zero pressure condition is essentially similar to the environment of choanoflagellates because they face no imposed pressure load from a canal system, and their flagella are able to create relatively high-volume flow rates in free space (or near surfaces) [19,23]. This may be one reason why the collar in choanoflagellates

Table 3. Pressure loss from the canal system (P_{ch}) (i.e. total pressure loss excluding contributions from within the choanocyte chambers) for different species of demosponges and one species of glass sponge (*Aphrocallistes vastus*). The relatively high-pressure loss in canals requires a high yield pump. Data extracted from [4], *[9], **[7].

species	P_{ch} (mmH_2O)
Cliona delitrix	5.803
Callyspongia vaginalis	2.676
Tethya californiana	0.233
Haliclona mollis	0.583
Neopetrosia problematica	0.867
*Aphrocallistes vastus**	0.855
*Haliclona urceolus***	0.436

lacks a dense mesh and instead, in some cases, has a fine ring of glycocalyx mesh encircling the microvilli [10]. But, of course, the main purpose of the collar is to act as a filter which is not impaired by a narrow ring that might serve a structural purpose.

3.3.3. Effect of the secondary reticulum

The secondary reticulum (R2) separates the high-pressure zone from the low-pressure zone as shown in figure 2*b* [11]. We therefore examine the hydrodynamic importance of R2 by removing this structure from the model (figure 2*c*) for an ideal case of zero imposed canal system pressure loss. Figure 7 shows the resulting velocity field in and around the choanocyte without the presence of R2. The flow rate through the collar is still similar to that without R2 (453 $\mu m^3\,s^{-1}$), but only ~13% of this flow is found to enter the domain from the prosopyle. The rest is a recirculating backflow from the inner part of the chamber around the collar. Consequently, the net pumping rate drops dramatically although without becoming zero. But in the real case with the presence of pressure resistance from the canals, the choanocyte pump would fail completely, leading to a reversed flow driven by the imposed pressure load.

Hydrodynamically, the three design elements, i.e. the R2, the glycocalyx mesh on the collar and the minimal gap between flagellar vane and collar, are crucial to the functionality of the choanocyte pump. As the glycocalyx mesh and the minimal gap are crucial to prevent leakage within individual choanocytes, the R2 reticulum is crucial for the assembly of choanocytes in the chamber to function in parallel, each being exposed to and able to deliver the required high pressure.

It remains to explain why the many choanocytes sit in a chamber with multiple prosopyles for inflow but a single apopyle for outflow. It is apparently not because of a favourable interaction because we have already shown that the hydrodynamic interaction between the choanocytes is negligible (table 1). Besides protection and being part of a larger organism, owing to high choanocyte density and structural rigidity, it also brings variety to their diet [11,14,22]. The reduced filter area for capturing bacteria has directed choanocytes to primarily become strong pumps with a relatively low filtration rate, which is compensated by the ability of leucon sponges to generate a strong inflow to the sponge, drawing

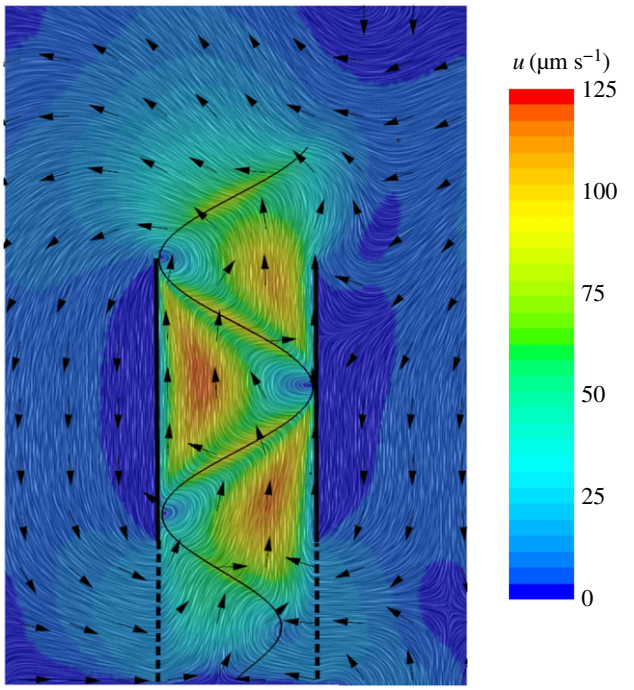

Figure 7. Velocity field in the choanocyte model of *Spongilla lacustris* without the secondary reticulum (R2 of figure 2*c*) for no imposed system pressure loss ($P_{ch} = 0$). While the flow through the collar exit is nearly the same as with the reticulum ($Q \sim 453\ \mu m^3\,s^{-1}$) the net flow rate leaving the choanocyte model is very low ($Q = 60\ \mu m^3\,s^{-1}$) because the pressure provided by the flagellum drives a strong backflow from the exit of the collar to its base as there is no reticulum to stop this. The colour bar and arrows (constant length) show the magnitude and direction of the velocity field, respectively. (Online version in colour.)

phytoplankton into long inhalant canals for capture, which contributes about 80% to their diet [24]. But the most compelling reason for near spherical choanocyte chambers is probably that they are a structurally practical and optimal design that can feature a two-pressure zone essential for parallel-coupled pumps that must yield high pressure. Here it is noted that, in both asconoid and sycoid sponges, choanocytes with cylindrical collars sit in close arrays on open surfaces, and there are no signs of reticula [12], which seems to agree with the fact that imposed flow resistance from the rather open canal structure is minimal.

3.4. Pump power and mechanical efficiency

The mechanical power expended by the beating motion of the flagellum in the choanocyte model (figure 2*c*), calculated from equation (2.4) for the normal case of BC 1 (in table 1), is $\mathcal{P}_{P,mech} = 12.6$ fW. For comparison the (reversible) useful pumping power received by the water flow at $Q = 454\ \mu m^3\,s^{-1}$ and an imposed system pressure loss of 1.0 mmH_2O plus the inner pressure drop of 0.95 mmH_2O through the inlet to the collar, a total of $P_T = 1.95\ mmH_2O$, amounts to $\mathcal{P}_{P,rev} = P_T Q = 8.68$ fW. The ratio of these powers represents the mechanical efficiency of the choanocyte pump model, $\eta_{mech} = \mathcal{P}_{P,mech}/\mathcal{P}_{P,rev} \approx 70\%$, which seems reasonable for a positive displacement pump. Our simulations also show η_{mech} to increase with decreasing gap width at higher values of pressure and flow rate, i.e. approaching an ideal displacement pump.

4. Conclusion

In this study, using detailed CFD simulations of flow in models of a choanocyte we find support for the hypothesis that the individual choanocyte is the basic pump unit in sponges. It can deliver the necessary high pressure because it operates as a leaky, positive displacement-type pump owing to the beating of its vaned flagellum in a collar, which is open at the base for inflow and sealed above by a tight glycocalyx mesh, and the leaking backflow is due to small gaps between the flagellum and collar. Our results contradict the earlier suggestion that the choanocyte chamber as a whole is the basic pump unit that delivers the needed high pressure. Finally, the calculated mechanical power of the flagellum gives reasonable values of mechanical efficiency of the model pump.

Data accessibility. This article has no additional data and all data for the numerical modelling are provided in the manuscript.

Authors' contributions. All authors designed the research. S.S.A., P.S.L., J.H.W. developed the model and and wrote the paper. H.U.R. provided biological advice on the pump model, model morphology and interpreting the results. S.S.A. performed the simulations.

Competing interests. We declare we have no competing interests.

Funding. This work was supported by a research grant no. (9278) from the VILLUM FONDEN.

References

1. Jørgensen CB. 1966 *Biology of suspension feeding*. Oxford, UK: Pergamon Press.
2. Riisgård HU, Larsen PS. 1995 Filter-feeding in marine macro-invertebrates: pump characteristics, modelling and energy cost. *Biol. Rev.* **70**, 67–106. (doi:10.1111/j.1469-185X.1995.tb01440.x)
3. Riisgård HU, Kumala L, Charitonidou K. 2016 Using the F/R-ratio for an evaluation of the ability of the demosponge *Halichondria panicea* to nourish solely on phytoplankton versus free-living bacteria in the sea. *Mar. Biol. Res.* **12**, 907–916. (doi:10.1080/17451000.2016.1206941)
4. Ludeman DA, Reidenbach MA, Leys SP. 2017 The energetic cost of filtration by demosponges and their behavioural response to ambient currents. *J. Exp. Biol.* **220**, 995–1007. (doi:10.1242/jeb.146076)
5. Reiswig HM. 1971 *In situ* pumping activities of tropical demospongiae. *Mar. Biol.* **9**, 38–50. (doi:10.1007/BF00348816)
6. Riisgård HU, Thomassen S, Jakobsen H, Weeks JM, Larsen PS. 1993 Suspension feeding in marine sponges *Halichondria panicea* and *Haliclona urceolus*: effects of temperature on filtration rate and energy cost of pumping. *Mar. Ecol. Prog. Ser.* **96**, 177–188. (doi:10.3354/meps096177)
7. Larsen PS, Riisgård HU. 1994 The sponge pump. *J. Theor. Biol.* **168**, 53–63. (doi:10.1006/jtbi.1994.1087)
8. Vogel S. 1994 *Life in moving fluids. The physical biology of flow*, 2nd edn. Princeton, NJ: Princeton University Press.
9. Leys SP, Yahel G, Reidenbach A, Tunnicliffe V, Shavit U, Reiswig H. 2011 The sponge pump: the role of current induced flow in the design of the sponge body plan. *PLoS ONE* **6**, e27787. (doi:10.1371/journal.pone.0027787)
10. Mah JL, Christensen-Dalsgaard KK, Leys SP. 2014 Choanoflagellate and choanocyte collar-flagellar systems and the assumption of homology. *Evol. Develop.* **16**, 25–37. (doi:10.1111/ede.v16.1)
11. Weissenfels N. 1992 The filtration apparatus for food collection in freshwater sponges (Porifera, Spongillidae). *Zoomorphology* **112**, 51–55. (doi:10.1007/BF01632994)
12. Leys SP, Eerkes-Medrano DI. 2006 Feeding in a calcareous sponge: particle uptake by pseudopodia. *Biol. Bull.* **211**, 157–171. (doi:10.2307/4134590)
13. Fjerdingstad EJ. 1961 The ultrastructure of choanocyte collars in *Spongilla lacustris* (l.). *Z. Zellforsch.* **53**, 645–657. (doi:10.1007/BF00339512)
14. Imsiecke G. 1993 Ingestion, digestion, and egestion in *Spongilla lacustris* (Porifera, Spongillidae) after pulse feeding with *Chlamydomonas reinhardtii* (Volvocales). *Zoomorphology* **113**, 233–244. (doi:10.1007/BF00403314)
15. Langenbruch P-F, Weissenfels N. 1987 Canal systems and choanocyte chambers in freshwater sponges (Porifera, Spongillidae). *Zoomorph.* **107**, 11–16. (doi:10.1007/BF00312124)
16. Mehl D, Reiswig HM. 1991 The presence of flagellar vanes in choanomeres of Porifera and their possible phylogenetic implications. *J. Zool. Syst. Evol. Res.* **29**, 312–319. (doi:10.1111/j.1439-0469.1991.tb00676.x)
17. Keller JB. 1964 Viscous flow through a grating or lattice of cylinders. *J. Fluid Mech.* **18**, 94–96. (doi:10.1017/S0022112064000064)
18. Silvester NR. 1983 Some hydrodynamic aspects of filter feeding with rectangular-mesh nets. *J. Theor. Biol.* **103**, 265–286. (doi:10.1016/0022-5193(83)90028-0)
19. Nielsen LT, Asadzadeh SS, Dölger J, Walther JH, Kiørboe T, Andersen A. 2017 Hydrodynamics of microbial filter feeding. *Proc. Natl Acad. Sci. USA* **114**, 9373–9378. (doi:10.1073/pnas.1708873114)
20. Walshaw AC, Jobson DA. 1962 *Mechanics of fluids*. London, UK: Longmans, Green.
21. Happel J, Brenner H. 1983 *Low Reynolds number hydrodynamics*, 2nd edn. Dordrecht, The Netherlands: Kluwer Academic Publishers.
22. Leys SP. 1999 The choanosome of hexactinellid sponges. *Invert. Biol.* **118**, 221–235. (doi:10.2307/3226994)
23. Asadzadeh SS, Nielsen LT, Dölger J, Andersen A, Kiørboe T, Larsen PS, Walther JH. 2018 Hydrodynamic functionality of the lorica in choanoflagellates. *J. R. Soc. Interface*.
24. Lüskow F, Riisgård HU, Solovyeva V, Brewer JR. In press. Seasonal changes in bacteria and phytoplankton biomass control the condition index of the demosponge *Halichondria panicea* in temperate danish waters. *Mar. Ecol. Prog. Ser.* (doi:10.3354/meps12785)